

# Effects of Spark Plasma Sintering Conditions on the Anisotropic Thermoelectric Properties of Bismuth Antimony Telluride

L. Han,<sup>a†</sup> S. H. Spangsdorf,<sup>a</sup> N. V. Nong,<sup>a†</sup> L. T. Hung,<sup>a</sup> H. N. Pham,<sup>a</sup> Y. Z. Chen,<sup>a</sup> A. Roch,<sup>b</sup>  
L. Stepien,<sup>b</sup> and N. Pryds<sup>a</sup>

<sup>a</sup> Department of Energy Conversion and Storage, Technical University of Denmark, Risø Campus, Roskilde, Denmark.

<sup>b</sup> Fraunhofer Institute for Material and Beam Technology (IWS), Dresden, Germany.

†e-mail of corresponding author: [ihan@dtu.dk](mailto:ihan@dtu.dk), [ngno@dtu.dk](mailto:ngno@dtu.dk)

## Table of Contents:

1. Supplement SEM images.
2. SPS sample cutting schematics.
3. Heat capacity  $C_p$
4. Metal droplets squeezed out of graphite die after SPS sintering
5. Calculations of Lorenz number
6. Sintering profiles of samples sintered with variable holding time, pressure, and ramp-rate.

## 1. Supplement SEM images

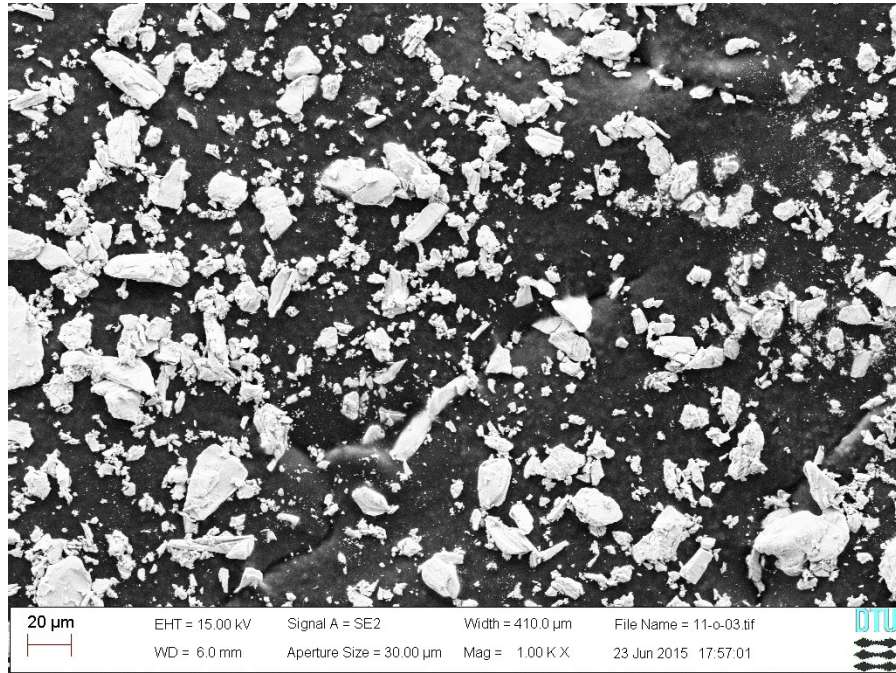


**Fig. S1** SEM of the Commercial  $\text{Bi}_{0.4}\text{Sb}_{1.6}\text{Te}_3$  powder

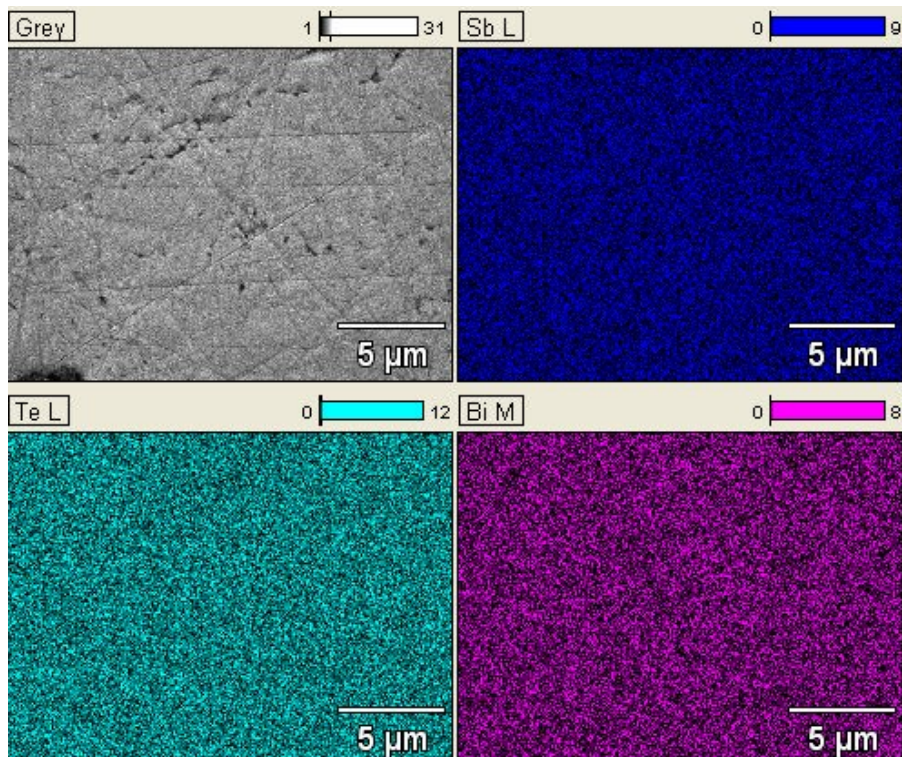


**Fig. S2** SEM-EDS element mapping of the specimen sintered by SPS at 653K.

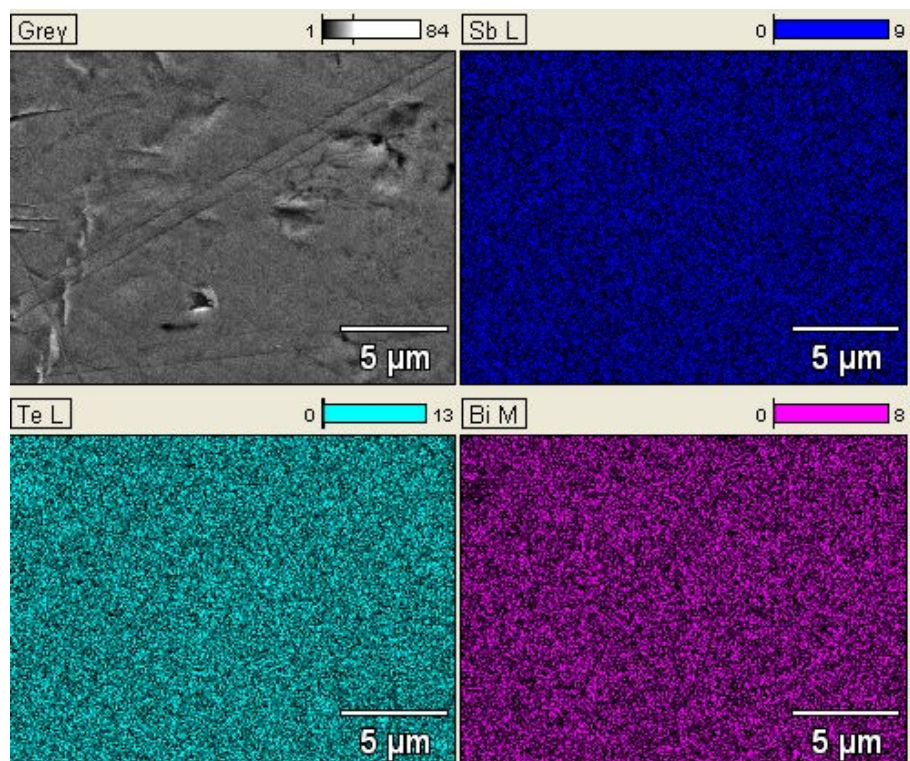


**Fig. S3** SEM-EDS element mapping of the specimen sintered by SPS at 773K.

## 2. SPS sample cutting schematics.

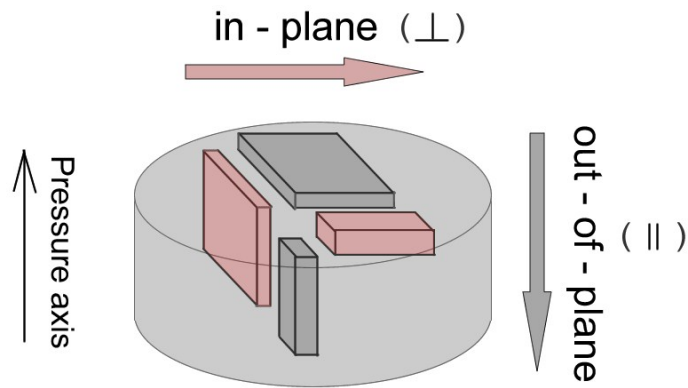


**Fig. S4** SPS sample cutting schematics. The red specimens were measured for in-plane thermoelectric properties, and the grey specimens were measured for out-of-plane thermoelectric properties.

## 3. Heat capacity $C_p$

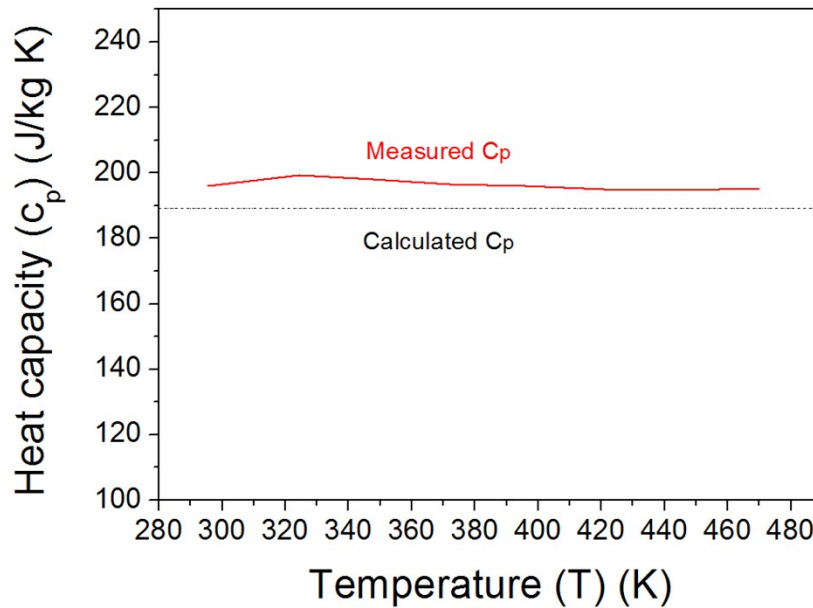


**Fig S5.** Temperature dependence of the specific heat at constant pressure for  $\text{Bi}_{0.4}\text{Sb}_{1.6}\text{Te}_3$  samples, the red line represents the measured value by DSC, and the dotted line represents the calculated values by Dulong-petit law.

#### 4. Metal droplets squeezed out of graphite die after SPS sintering



**Fig. S6** Spilled droplets squeezed out of graphite die after SPS sintering at 723 K (left) and 773 K (right).

#### 5. Calculations of Lorenz number $L_o$

According to the measured  $n$  and estimated  $m^*$  values, a simple parabolic band model can be applied by employing the following equations:

$$F_\lambda(\xi) = \int_0^\infty \frac{x^\lambda dx}{1 + \text{Exp}(x - \xi)} \quad (\text{S1})$$

$$L_o = \left( \frac{k_B^2}{q^2} \right) (3F_0 F_2 - 4F_1^2) / F_0^2 \quad (\text{S2})$$

where  $F_\lambda(\xi)$  is the Fermi integral and  $\xi$  is the reduced electrochemical potential.  $\lambda$  is a scattering parameter and 0 is assumed for acoustic phonon scattering, 1 for optical phonons scattering, and 2 for ionized impurity scattering.  $k_B$  is the Boltzmann constant,  $q$  is the unit charge of electron.  $\xi$  is calculated from the measurement Seebeck coefficient ( $S$ ) using the following equation:

$$S = -\frac{k_B}{q} \left[ \frac{(2 + \lambda)F_{\lambda+1}}{(1 + \lambda)F_{\lambda}} - \xi \right] \quad (\text{S3})$$

**6. Sintering profiles of samples sintered with variable holding time, pressure, and ramp-rate.**

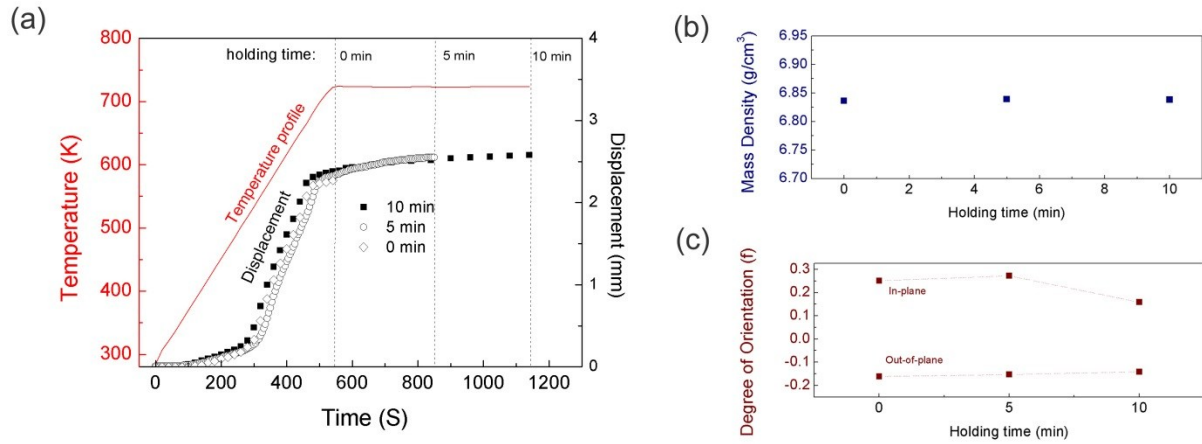


**Fig. S7.** (a) Sintering profile for SPS sintering with variable holding time. (b) Mass density of the samples as a function of holding time. (c) Degree of orientation as a function of holding time.

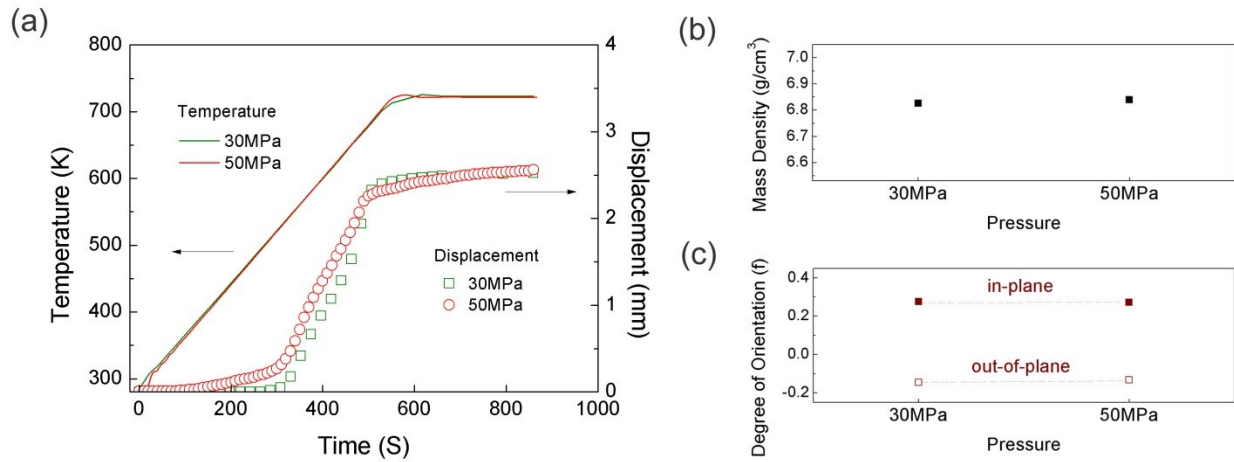


**Fig. S8** (a) Sintering profile for SPS sintering with variable pressure. (b) Mass density of the SPS sintered samples with variable uniaxial pressure. (c) Degree of orientation as a function of uniaxial pressure.

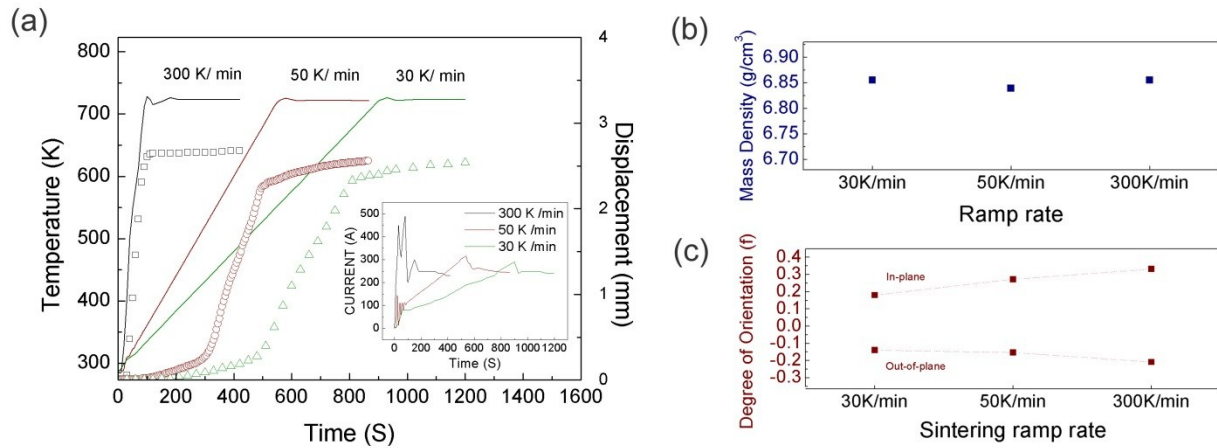


**Fig. S9** (a) Sintering profile for SPS sintering with variable ramp-rate. The inset shows the current profile during SPS sintering. (b) Mass density of the samples sintered with variable ramp-rate. (c) Degree of orientation of the samples sintered with variable ramp-rate.